AIAA JOURNAL
Vol. 42, No. 3, March 2004

Broadband Self-Noise from Loaded Fan Blades

Michel Roger*
Ecole Centrale de Lyon, 69134 Ecully, France
and
Stéphane Moreau†
Valeo Motors and Actuators, 78321 La Verrière, France

An experimental investigation and analytical modeling were conducted of the broadband self-noise radiated by an industrial cambered airfoil embedded in an homogeneous flow at low Mach number. The instrumented airfoil is placed at the exit of an open jet anechoic wind tunnel. Sound is measured in the far field at the same time as the statistical properties of the wall pressure fluctuations close to the trailing edge. Three different flows with different statistical behaviors are investigated by changing the angle of attack, namely, the turbulent boundary layer initiated by a leading-edge separation, the nearly separated boundary layer with vortex shedding at the trailing edge, and the laminar boundary layer with Tollmien–Schlichting waves. The far-field spectrum is related to the spectrum and spanwise correlation length of the wall pressure fluctuations. Simple statistical models based on Howe's theory and on an extension of the original Amiet's theory show a good agreement with the experimental results. They provide helpful tools to predict the self-noise from subsonic fans in an industrial context.

Nomenclature

b	=	nondimensional parameter in Corcos's model
c	=	airfoil chord length
c_0	=	speed of sound
f	=	frequency
I	=	total radiation integral, $I_1 + I_2$
I_1	=	main trailing-edge radiation integral
I_2	=	leading-edge backscattering radiation integral
K_2	=	non-dimensional aerodynamic wave number in the spanwise direction
k	=	acoustic wave number
L	=	wetted spanwise extent of the trailing edge
$l_y(\omega)$	=	spanwise correlation length
M	=	Mach number based on the flow speed, U_0/c_0
M_c	=	Mach number based on the convection speed of the disturbances, U_c/c_0
(R, θ)	=	polar coordinates of the observer
Re_c	=	Reynolds number based on the airfoil chord length
S_{pp}	=	acoustic power spectral density
U_c	=	convection speed
U_0	=	flow speed
$\boldsymbol{x}$	=	observer position
$\{x + iy\}^c$	=	corrected complex number, $x + i \epsilon y$
α	=	profile trailing-edge inclination angle
α_g	=	angle of attack with respect to the camber line at the leading edge
γ^2	=	coherence function
δ_S	=	thickness of the suction side boundary layer at the trailing edge
ϵ	=	corrective factor in leading edge backscattering radiation integral
η	=	spanwise distance between two sensors
Θ	=	microphone angle
Φ_{pp}	=	wall pressure power spectral density
ω	=	radian frequency

Received 17 August 2001; presented as Paper 2002-2460 at the AIAA/CEAS 8th Aeroacoustics Conference, Breckenridge, CO, 3 June 2002; revision received 9 July 2003; accepted for publication 14 July 2003.

*Professor, Laboratoire de Mécanique des Fluides et Acoustique. Member AIAA.

†Research Engineer and Research and Development Manager, Engine Cooling Fan Systems Core Competencies Group. Member AIAA.

I. Introduction

An airfoil embedded in a quiet flow radiates noise, for any flow velocity and angle of attack, due to vortical disturbances developing in the boundary layers. This experimental evidence holds whatever the precise nature of the disturbances (random or organized) might be. Only the spectral and amplitude characteristics of the sound field are modified. Turbulent boundary layers, attached or separated at the trailing edge, generate broadband noise, whereas laminar unstable boundary layers are known to be responsible for the emission of an intense whistle. Note that the same physical process is basically involved in all cases: Vortical disturbances are partially converted into acoustical ones as soon as they are convected past a geometrical discontinuity, such as the trailing edge. This fundamental mechanism is referred to as trailing-edge noise or self-noise.

Airfoil self-noise is considered to be a significant part of the broadband noise emitted by lifting surfaces, such as wings and rotating fan blades. It defines the minimum amount of noise from a fan in the absence of installation effects. Moreover, in the case of wind turbine blades, it is the only significant nuisance in the range of human hearing.

The study of trailing-edge noise has received much attention mainly in the late 1970s and early 1980s. Experimentally, it involved measurements of wall pressure fluctuations and far-field sound on two-dimensional mock-ups of various aerodynamic airfoils in free-jet anechoic wind tunnels.[1–3] Theoretical ad hoc models were also developed at the same time.[4–6] More recently, the available experimental data have been used to validate sophisticated numerical prediction methods for trailing-edge aeroacoustics, such as large-eddy simulation (LES).[7–10] Yet, even though these methods are powerful, they do not provide a simple and reliable tool that could be used in an industrial design cycle. Such a tool implies two mains steps, highlighted in the present study. First, analytical formulations based on the acoustic analogy approach are developed. Second, experimental validation is presented on an airfoil shape that can be industrially manufactured. Self-noise is investigated here on a controlled diffusion (CD) airfoil designed by Valeo Motors and Actuators, with rounded leading and trailing edges. The camber angle is about 12 deg, which allows for the assessment of loading effects, and the maximum relative thickness is 4%.

The next section is devoted to the analytical statistical models of trailing-edge noise. In particular, the actual airfoil chord length is accounted for in the formulation. The primary work of Amiet[5]

is completed by the introduction of a leading-edge backscattering correction. The experimental setup and related topics for the model are presented in Sec. III. In Sec. IV the main experimental results for three different flow regimes are given. Then the theoretical formulas are checked against the measured transfer function between the wall pressure spectra and the far-field noise in Sec. V.

II. Analytical Formulations

The theoretical problem of the acoustic scattering of vortical boundary-layer disturbances convected past a trailing edge has been thoroughly addressed in the literature, among others by Ffowcs Williams and Hall,[4] Amiet,[5] and Howe.[6] Different approaches can be identified, depending on the way both noise generation and noise propagation are handled. A first difference arises in the aerodynamic quantity that is related to the acoustic pressure in the far field. In the primary work of Ffowcs Williams and Hall[4] applied by Wang and Moin[7] or Manoha et al.,[11] Lighthill's equation is formally solved using the half-plane Green's function. The acoustic pressure is then expressed naturally in terms of vortical velocity components around the trailing edge. The other approaches[5,6] generally relate the statistics of the far-field acoustic pressure directly to the statistics of the aerodynamic wall pressure at some distance upstream of the trailing edge. This is taken for granted here, even though using the wall pressure as an equivalent acoustic source has given rise to controversy because the origin of the sound is in the vortical velocity field. A second difference is the way the airfoil geometry is accounted for in the formulation. Most studies are based on the assumption of a rigid half-plane.[4,6] It is argued that the scattering process is localized close to the trailing edge and is nearly independent of what happens farther upstream. For instance, according to Howe's theory[6] (also see Ref. 2), the far-field noise in the midspan plane can be related to the wall pressure spectrum taken in the close vicinity of the trailing edge and the spanwise correlation length as

$$S_{pp}(\boldsymbol{x},\omega)=\left[\frac{\sqrt{2}\,\sin(\theta/2)}{\pi R}\right]^2 M_c\,\frac{L}{2}\,\Phi_{pp}(\omega)\,l_y(\omega) \qquad (1)$$

This expression holds at moderate Mach number, assuming a full Kutta condition, and with the origin at the trailing edge.

Equation (1) emphasizes that the trailing-edge radiation exhibits the cardioid pattern expressed by the $\sin^2(\theta/2)$ function. The chord length of a real airfoil is large practically when compared to the aerodynamic wavelengths associated with boundary-layer eddies. However, it may not be large with respect to the acoustic wavelengths. As a result, the earlier half-plane assumption is not consistent at the low frequencies of interest in fan noise applications, for which the blade chord is of the same order of magnitude, and eventually smaller, than the acoustic wavelength. This can be quantified by comparing the nondimensional frequency $k\,c$ scaling the acoustic wave number k to the airfoil chord length c, to unity. For instance, $k\,c$ covers the range 0.12–12 for typical automotive cooling fan blades. The often ignored leading-edge backscattering has two effects. The first one is a contribution to the induced unsteady lift distribution. The second one is a modification of directivity. In fact, in the case of an airfoil with finite chord length, the upstream radiation is zero, with two main lobes inclined forward, as clearly shown by numerical simulations.[12] The aforementioned cardioid behavior of the half-plane theories is only recovered at very high frequencies and can be seen as an asymptotic trend. These features must be reproduced by any method aimed at predicting both frequency distribution and directivity. Strictly speaking, trailing-edge noise radiation should be obtained from the Green's function tailored to the actual airfoil shape in a flowfield, rather than from a half-plane one (see Ref. 13).

For industrial purposes, moderate airfoil thickness and camber can be neglected in the sound radiation mechanism. The main assumption here is that the flow does depend on these parameters, whereas the acoustic radiation itself rather involves a global surface effect. The airfoil is then assimilated to a flat plate with zero thickness and finite chord length embedded in a uniform flow.

At very low Mach numbers, the effects of the main flow on sound propagation can be neglected, allowing some simplifications. Howe[14] recently proposed a Green's function tailored to a finite chord length, dedicated to trailing-edge noise sources at very low Mach number. A slightly different approach is used here following Amiet.[5] Instead of deriving a Green's function in an explicit form, we deduce the radiated field from the incident wall pressure field at the trailing edge by invoking the solution of an equivalent wave scattering problem. The principle of the derivation is given in Ref. 15 and is just outlined here. The incident pressure field is first split into sinusoidal pressure gusts. A gust convected past the trailing edge is scattered according to the Kutta condition and induces a disturbance pressure field on the surface. This field acts as equivalent acoustic sources in the sense of the acoustic analogy. The diffraction by the surface is automatically accounted for in the formulation.

The standard solution was first proposed by Amiet to handle the problem of the noise from turbulence impinging on an airfoil[16] and then extended to trailing-edge noise.[5] It deals with the basic scattering of waves by the edge of a half-plane and should be applied in an iterative way (Schwarzschild's technique). The main trailing-edge scattering is determined assuming that the airfoil surface extends toward infinity in the upstream direction. Amiet[5] reduced the formulation to this first evaluation for two-dimensional gusts and calculated the radiated sound field by integrating the induced surface sources over the actual chord length. When his result is specified to low Mach numbers such that it can be compared to Eq. (1), it becomes

$$S_{pp}(\boldsymbol{x},\omega)=(\sin\theta/2\pi R)^2(kc)^2(L/2)|I|^2\Phi_{pp}(\omega)l_y(\omega) \qquad (2)$$

with I a radiation integral involving both the freestream velocity and the convection speed as parameters.

However, the real condition in front of the airfoil is not satisfied by the original expression of I given by Amiet.[5] The main theoretical contribution in Ref. 15 reproduced here is a corrected form of I that accounts for a leading-edge correction. It is reduced to low Mach numbers, ignoring convection effects on sound radiation. A first but crude approximation of the correction has been proposed by Sabah and Roger.[17] The more accurate approximation in Ref. 15 compares favorably with Howe's results.[14] A three-dimensional extension of Amiet's result[5] has also been achieved by taking three-dimensional gusts that can be factorized to apply the Schwarzschild's technique.

The final result is given in terms of the contributions of each iteration to the radiation integral involved in formula (2), $I=I_1+I_2$. The main trailing-edge contribution[5] is

$$I_1=-(e^{2iC}/iC)\left\{(1+i)\sqrt{B/(B-C)}e^{-2iC}E^*[2(B-C)]+1-(1+i)E^*(2B)\right\}$$

with

$$B=\bar{K}_1+(1+M)\bar{\kappa},\qquad C=\bar{K}_1-\bar{\mu}(x_1/S_0-M)$$

$$\bar{\kappa}^2=\bar{\mu}^2-\bar{K}_2^2/\beta^2,\qquad \bar{\mu}=\bar{K}M/\beta^2,\qquad \beta^2=1-M^2$$

$$\bar{K}=K(c/2),\qquad K=\omega/U_0,\qquad \bar{K}_1=\omega c/2U_c=\xi\bar{K}$$

$\bar{K}_2$ is set to zero for the present application. Similarly, the leading-edge backscattering correction is

$$I_2=H(\{e^{4i\bar{\kappa}}[1-(1+i)E^*(4\bar{\kappa})]\}^c-e^{2iD}+i[D+\bar{K}+(M-1)\bar{\kappa}]G)$$

with

$$H=\frac{(1+i)e^{-4i\bar{\kappa}}(1-\Theta^2)}{2\sqrt{\pi}(\alpha-1)\bar{K}\sqrt{B}},\qquad D=C-(\bar{K}_1+(M-1)\bar{\kappa})$$

$$G=(1+\epsilon)e^{i(2\bar{\kappa}+D)}\frac{\sin(D-2\bar{\kappa})}{D-2\bar{\kappa}}+(1-\epsilon)e^{i(-2\bar{\kappa}+D)}\frac{\sin(D+2\bar{\kappa})}{D+2\bar{\kappa}}$$
$$+\frac{(1+\epsilon)(1-i)}{2(D-2\bar{\kappa})}e^{4i\bar{\kappa}}E^*(4\bar{\kappa})-\frac{(1-\epsilon)(1+i)}{2(D+2\bar{\kappa})}e^{-4i\bar{\kappa}}E(4\bar{\kappa})$$
$$+\frac{e^{2iD}}{2}\sqrt{\frac{2\bar{\kappa}}{D}}E^*(2D)\left[\frac{(1+i)(1-\epsilon)}{D+2\bar{\kappa}}-\frac{(1-i)(1+\epsilon)}{D-2\bar{\kappa}}\right]$$

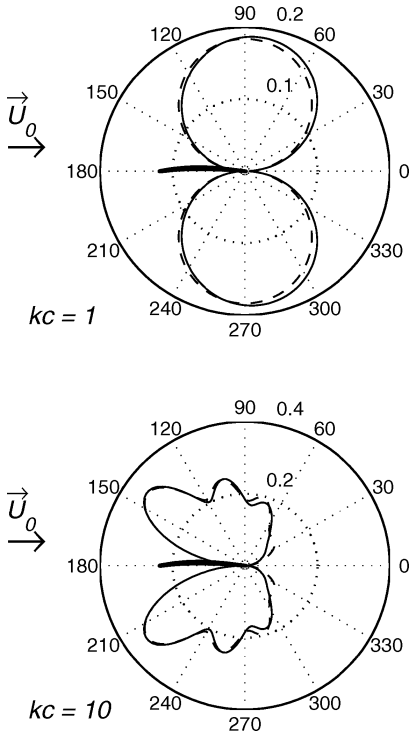

Fig. 1 Predicted directivity patterns for $M = 0.05$: - - - -, main trailing-edge radiation and ——, total radiation.

$$\epsilon = \left(\sqrt{1 + \frac{1}{4\bar{\kappa}}}\right)^{-1}, \qquad E^*(x) = \int_0^x \frac{e^{-it}}{\sqrt{2\pi t}}\,\mathrm{d}t$$

Typical directivity patterns are plotted in Fig. 1 for two different values of the reduced wave number kc. The difference between the main trailing edge and the full solutions corresponds to the leading-edge correction. As expected, the former correction is only important at low reduced frequencies, for example, for kc of order 1 and less. It can be significant for fans with small blade chords such as the automotive fans. As shown in Fig. 2, these sound directivities are in very good agreement with Howe's solution valid for low Mach numbers.[14] As frequency increases, the two main lobes are inclined upstream and tend to the asymptotic cardioid pattern with secondary lobes.

Both Eqs. (1) and (2) result from the Corcos's hypothesis of a factorization of the frequency-wave number spectrum of the wall pressure fluctuations. In the special case of a fully turbulent boundary layer over a flat plate with zero pressure gradient, $l_y(\omega)$ is deduced from Corcos's model[18] yielding

$$l_y(\omega) = bU_c/\omega \tag{3}$$

In the case of a curved surface such as an airfoil, the precise value of $l_y(\omega)$ can be different from the result of Eq. (3).

The main objective of the present study is to check the consistency of formulas (1) and/or (2) in different flow conditions corresponding to different configurations, to assess their usefulness for broadband noise prediction applied to subsonic fans. The experiment may answer the question whether the wall pressure field can be used to compute the far-field sound. Furthermore, it may indirectly help to assess the fulfillment of the unsteady Kutta condition.

Because S_{pp} and Φ_{pp} are measured simultaneously on the same acquisition system, the analytical formulation is simply evaluated by the ratio S_{pp}/Φ_{pp}. According to Eq. (1), this transfer function is proportional to $l_y(\omega)$, which leads to a decrease inversely proportional to frequency when Corcos's model is applied. According to Eq. (2), it is proportional to $l_y(\omega)$ times the product $|kcI|^2$, the

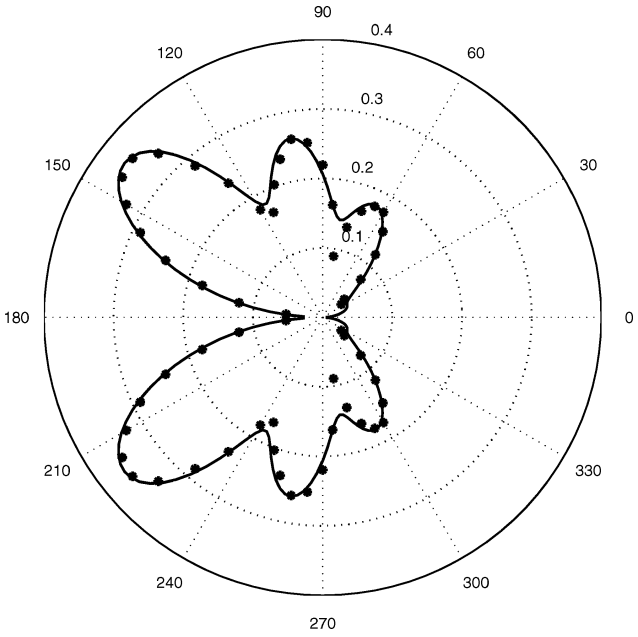

Fig. 2 Directivity plot for $kc = 10$ and $M = 0.05$: symbols, Howe's model and ——, present model.

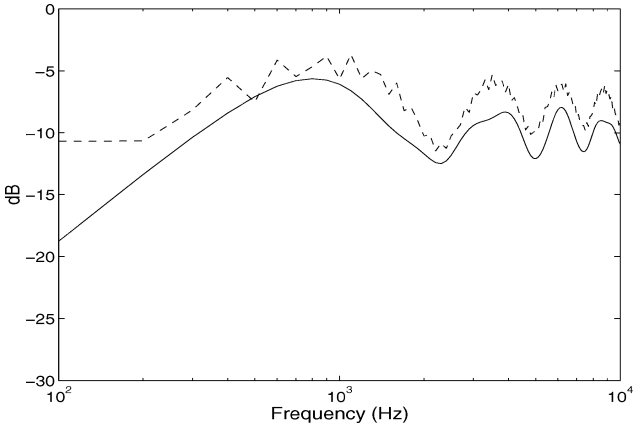

Fig. 3 Amiet's radiation factor $|kcI|^2$ for two speeds, $c = 13.6$ cm: – – –, $U_0 = 30$ m/s ($Re_c = 2.9 \times 10^5$) and ——, $U_0 = 16$ m/s ($Re_c = 1.6 \times 10^5$).

latter being only related to the dipolar nature of the source and the radiation integral over the airfoil surface. Both the half-plane and the finite-chord formulas are easily compared by the ratio

$$\frac{\text{Eq. (2)}}{\text{Eq. (1)}} = \left[\frac{\sin\theta}{\sin(\theta/2)}\right]^2 \frac{|kcI|^2}{8M_c} \tag{4}$$

Because of its importance in formula (2), the nondimensional factor $|kcI|^2$ is plotted in decibels as a function of frequency in Fig. 3. For a given angle of radiation, it is an oscillating function over the frequency range of interest, around a constant value. As a result, the ratio (4) is mainly a function of angle θ, which makes both formulations quite similar.

$\Phi_{pp}(\omega)$ and $l_y(\omega)$ can be deduced from wall pressure measurements by a distribution of spanwise sensors. As shown in Ref. 19, $l_y(\omega)$ is related to the coherence function γ^2 between signals measured by two sensors η-apart spanwise and with the same chordwise location. It can be evaluated analytically provided that the decrease of γ^2 with η is interpolated by an exponential function. The convection speed U_c is calculated from the phase diagrams of the measured cross-spectral densities between two points close to each other in the streamwise direction, in the vicinity of the trailing edge.

III. Experimental Setup

The experimental validation of formulas (1) and (2) is far more convincing if boundary-layer flows with significantly different statistical parameters are investigated. Opposite trends are then needed associated with small and large spanwise coherence scales, on the one hand, and with narrowband and wideband frequency distributions on the other hand. This is the reason why the turbulent attached flow and the laminar boundary layer with Tollmien–Schlichting instability waves (T–S) are of primary interest. Furthermore, most fan blades partially operate at off-design conditions for which flow separation or boundary-layer growth occurs in the trailing-edge area, making the question of trailing-edge noise from loaded airfoils another important case to be investigated. All preceding configurations or equivalent conditions are obtained here with the same Valeo airfoil just by changing the angle of attack in the experimental setup. The main features of the flow have been visualized by brushing a liquid paraffin with carbon particles on the airfoil surface and by exploring the streamlines around the trailing edge with tufts.

The experiment has been performed at the Laboratoire de Mécanique des Fluides et Acoustique de l'Ecole Centrale de Lyon (ECL-LMFA). The experimental setup is shown schematically in Fig. 4. The airfoil is maintained between horizontal side plates flush mounted at the nozzle of an open jet anechoic wind tunnel. The reference angle for the airfoil position is the geometrical angle of attack α_g with respect to the mean camber line at the leading edge. The residual turbulence level of the wind tunnel is less than 1%, ensuring reliable self-noise studies. The airfoil chord and span are 13.6 cm (5 ft) and 30 cm (11.9 ft), respectively, and correspond to the nozzle jet width and height. Acoustic pressure is measured in the far field in the midspan plane thanks to a standard BK 1/2-ft microphone on a rotating arm, 1.3 m (4 ft) distant from the mock-up trailing edge. The microphone angle Θ is now referenced to the direction of the incident flow. The unsteady wall pressure on the airfoil surface is measured using remote microphone probes (RMP); such a probe is made with a spanwise flush-mounted capillary tube and a pin hole at the measuring point. The capillary is progressively enlarged outside the mock-up till a small Electret microphone can be flush mounted. A long polyvinylchloride (PVC) tube is connected to the outer end of the capillary to attenuate longitudinal waves. The RMP measures both the mean pressure (leading to the pressure coefficient) and the unsteady pressure within the frequency range 20 Hz–25 kHz: Pressure fluctuations induced on the surface by either turbulent or unstable laminar boundary layers force acoustic waves inside the capillary that are received by the microphone. Technological details and correction for attenuation and reflection effects inside the probes are given by Pérennès and Roger.[20] As a matter of fact, the RMP is an acoustical sensor or an aerodynamical sensor depending on the nature of the boundary-layer flow. If the boundary layer is developing in a favorable pressure gradient, it is laminar with no oscillations; the probe is a near-field acoustical sensor. In contrast, as soon as the boundary layer oscillates, it is an aerodynamical sensor because vortical disturbances are an order of magnitude higher than acoustic disturbances. Furthermore, acoustic disturbances are highly correlated over the airfoil surface, whereas aerodynamic disturbances have much smaller correlation scales.

A near-field wall pressure acoustic signal also looks like a far-field signal; in contrast, the aerodynamic wall pressure signal generally exhibits different spectral features at a far higher level. Finally, the aerodynamic nature of the wall pressure field can be confirmed by evaluating the convection speed. Only the clearly identified aerodynamic information has been retained in the present analysis. There are 21 measuring points distributed over the airfoil, mostly along the chord line at midspan on the suction side. Four of them have the same chordwise location 3 mm from the trailing edge but at different locations along the span for spanwise coherence measurements. Probes are concentrated at the leading edge and at the trailing edge to capture both the laminar separation bubble observed for some angles of attack with this airfoil and the turbulent vortex shedding regime near the trailing edge.

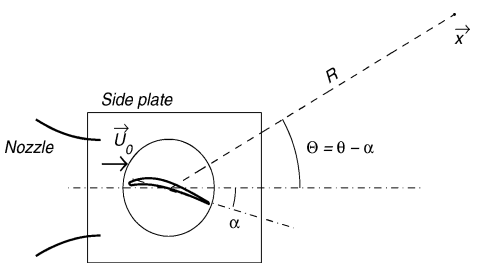

Fig. 4 ECL-LMFA experimental setup and geometrical parameters.

Because the nozzle width is almost equal to the chord length, any lifting angle of attack induces a significant mean flow deflection. The aerodynamic effect is twofold. On the one hand, the effective net load is much less than the load that the airfoil would experience in an infinite stream with the same angle of attack. On the other hand, the typical pressure coefficient distribution measured on the setup cannot be fit by any equivalent free air distribution by changing the angle of attack. Though such a possible correction is mentioned by Brooks et al.[21] for a NACA0012 airfoil, the same is not achievable with the present airfoil. Moreover, additional recent two-dimensional Reynolds-averaged Navier–Stokes (RANS) computations[22] have shown that the actual pressure coefficient in the wind tunnel is close to the one that would be obtained with the same airfoil in a cascade configuration. This installation effect may be ignored here because the far-field noise and the wall pressure are measured in the same experiment to evaluate the transfer function discussed in Sec. III. The incident flow velocity was varied from 16 to 41 m/s, corresponding to a chord-based Reynolds number of 1.4×10^5–3.5×10^5.

IV. Main Results

Because broadband trailing-edge noise provides the minimum airfoil noise levels, far-field acoustic signals must be carefully compared with the background noise contribution. The sources of background noise are defined as the noise when the airfoil is removed but in the presence of flow between the side plates. The results used here to relate the acoustic pressure to the wall pressure measurements are corrected according to the following procedure. Background noise sources are most likely uncorrelated with trailing-edge noise sources on the airfoil. Furthermore, they are assumed to be the same with and without the airfoil, which is only approximate due to the flow deflection effect. Then, if M_1 and M_2 denote the measured levels in decibels corresponding to background noise and the noise with the mock-up installed, airfoil trailing-edge noise in decibels is extracted using the formula

$$|S_{pp}|_{\mathrm{dB}} = M_2 + 10\log_{10}(1 - 10^{(M_1 - M_2)/10})$$

M_2 exceeds M_1 by a typical amount of 10 dB in the frequency range of interest, ensuring reliable measurements for radiation angles far enough from the airfoil wake ($|\theta| > 20$ deg). In view of the very small differences observed in successive tests, refraction is responsible for the major uncertainties in these measurements. The refraction due to the shear layers surrounding the mock-up and originating at the nozzle lips has been accounted for using Amiet's correction formulas.[23] It is small here due to the values of the Mach number (less than 0.1) and the relative width of the wind-tunnel flow. The maximum refraction angle and amplitude corrections are 10 deg and 1.5 dB, respectively. These are only error estimates because Amiet's formulas hold for a parallel shear layer and the present deflected jet boundary is curved. Wall pressure spectra could be reproduced with an accuracy below 1 dB.

A. Turbulent Boundary Layer

Results for Φ_{pp} and S_{pp} at $\Theta = 90$ deg are reported in Fig. 5 for the Valeo airfoil at an angle of attack $\alpha_g = 13$ deg and for a flow velocity of 16 m/s. In this case, a statistical behavior corresponding to a developed turbulent flow is observed on the suction side in the trailing-edge region. Though surprising in view of the high angle of attack, such a flow is allowed by the strong stream deflection in the

Table 1 Characteristic parameters of airfoil self-noise for different experimental conditions

Airfoil/reference	Constant $1/b$	Convection speed, U_0	Flow speed, m/s	Chord length, cm
Flat plate/Corcos[18]	0.714	0.7	$U_0 = 69$	Any
Flat plate/Amiet[5]	0.476	0.8	$U_0 = 102$	Any
NACA0012/Brooks and Hodgson[2]	0.62	0.6	$U_0 = 38.6$	61
	0.58	0.6	$U_0 = 69.5$	61
NACA0012/Garcia and Gérard[3]	0.9	0.8	$U_0 = 60$	50
Airbus A320/Pérennès and Roger[20]	0.28	0.65	$U_0 = 80$	30
Present paper Valeo CD	0.67 (13 deg)	0.6	$U_0 = 16$	13.6
	Ad hoc model (5.5 deg)	0.7		
	Ad hoc model (−5 deg)	0.65		

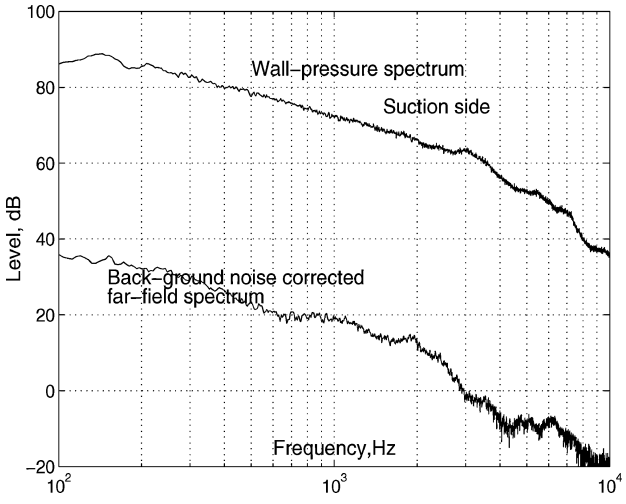

Fig. 5 Surface and far-field spectra for the turbulent boundary layer, $\alpha_g = 13$ deg, and $U_0 = 16$ m/s ($Re_c = 1.6 \times 10^5$).

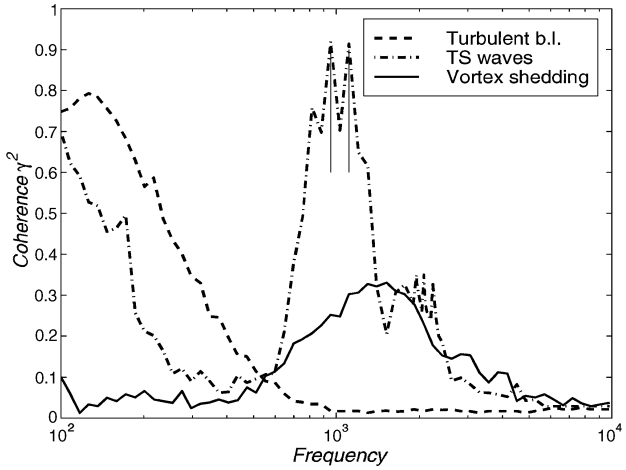

Fig. 6 Coherence plots for the three different flow regimes.

setup. It is initialized by an extended leading-edge separation bubble. Within the frequency range in which airfoil noise clearly dominates background noise, extending from 400 Hz to 10 kHz, wall pressure and acoustic spectral envelopes are quite closely related, indicating a clear cause–effect relationship.

An example of a coherence plot is given in Fig. 6, where the same information for the subsequent flow regimes is superimposed for comparison. The spanwise correlation length, small for turbulent boundary layers, is only partially measured by the trailing-edge set of spanwise RMP. As suggested by the results of Fig. 7, the coherence between the probes decreases with both frequency and separation. This is in relative accordance with Corcos's model,[18] provided that the coefficient b is adjusted to the measurements. The observed value here is $b = 1.5$, very close to the reference value for

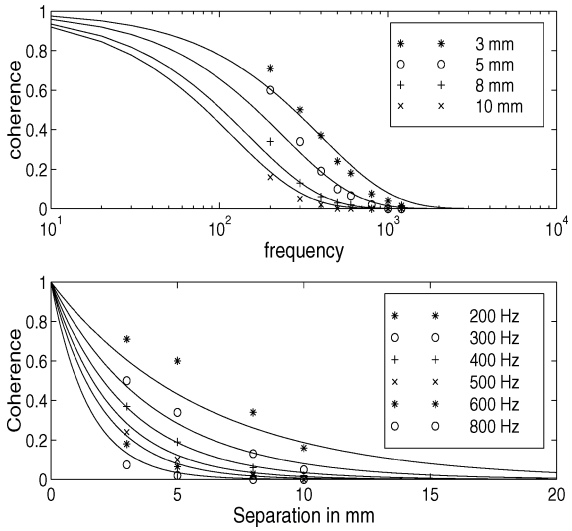

Fig. 7 Justification of a Corcos's model for the turbulent boundary layer, $\alpha_g = 13$ deg and $U_0 = 16$ m/s ($Re_c = 1.6 \times 10^5$).

a boundary layer over a flat plate. It is compared to previous measurements along with the convection speed in Table 1. Furthermore, it has been verified that the wall pressure field is homogeneous in the streamwise, as well as in the spanwise, direction. From the trailing edge to several centimeters upstream of it, the wall pressure spectra can be superimposed almost perfectly. At these flow conditions, the boundary layer at the rear part of this airfoil behaves in the same way as the one over an ideal flat plate with zero pressure gradient because the airfoil is almost stalled with a nearly constant pressure on the suction side.

B. Laminar Boundary Layer with TS Waves

A laminar boundary layer initially develops on an airfoil in homogeneous inflow conditions for which the residual turbulence rate is less than 1 or 2%. At low chord-based Reynolds numbers, typically below 2×10^5, and for moderate angles of attack, the boundary layer becomes unstable at a given point referred to as point P here, locus of a change of sign of the streamwise pressure gradient, but may not transition to turbulence up to the trailing edge. This is the case on the present CD airfoil where the Reynolds number is 1.6×10^5 for a velocity of 16 m/s and an angle of attack $\alpha_g = -5$ deg. The resulting T–S waves grow exponentially along the chord and radiate noise when scattered by the trailing edge.

This T–S wave radiation is shown in Fig. 8. It is characterized by a primary rather narrowband hump, on the one hand, and by discrete frequencies superimposed on it, on the other hand. A secondary similar pattern appears at twice the peak frequencies due to distortion. These special features exist because the aerodynamical oscillations within the boundary layer and the related sound field remain correlated over the whole airfoil surface of interest and the surrounding area. As a result, the sound waves propagating upstream are able to force the instability waves at their starting point P, leading to self-sustained oscillations with high amplitude at privileged

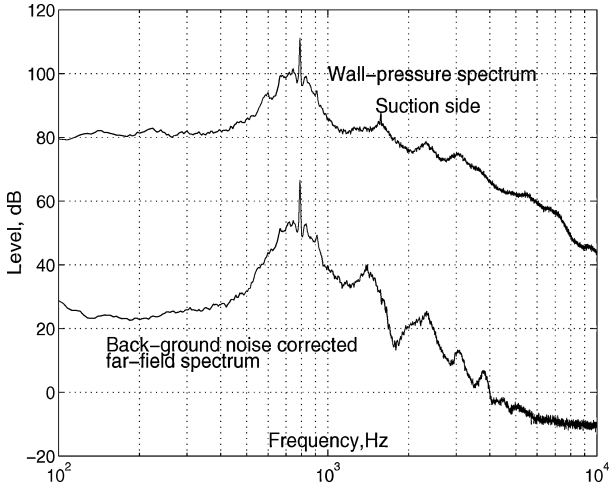

Fig. 8 Wall pressure and far-field spectra for T–S wave radiation, $\alpha_g = -5$ deg and $U_0 = 16$ m/s ($Re_c = 1.6 \times 10^5$).

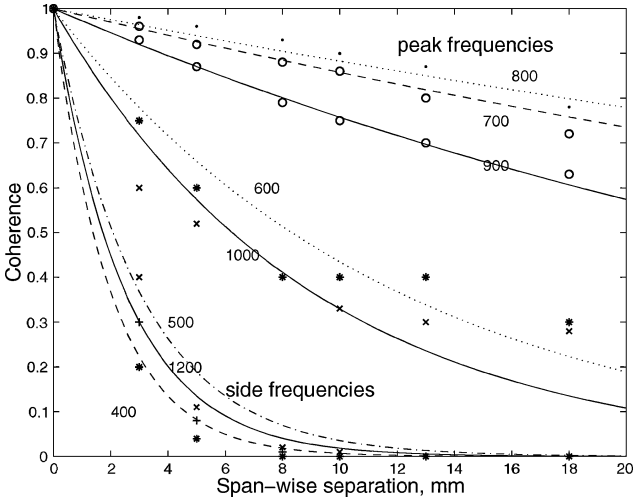

Fig. 9 Coherence decay for T–S waves, $\alpha_g = -5$ deg and $U_0 = 16$ m/s ($Re_c = 1.6 \times 10^5$).

frequencies.[24,25] These tones, for which a favorable phase-lock occurs during the acoustic feedback, lead to a strong amplification of about 10 dB here, compared to the natural T–S wave amplitude in the absence of backreaction. Flow visualizations have shown that a thin laminar separation bubble is formed at the trailing edge, in accordance with the observations made by McAlpine et al.[26] but not with the ones by Arbey and Bataille,[24] for which the boundary layer remained attached. As shown by the phase diagrams, not plotted here, the induced pressure on the surface is convected in the streamwise direction, despite the flow separation. This is certainly because the oscillations of the bubble shear layer remain close to the surface. This discrete frequency radiation has also been investigated in the literature on the basis of other physical arguments involving laminar separation at trailing edge or oscillations in the wake, among others by McAlpine et al.[26] and Tam.[27]

Coherence measurements exhibit a specific behavior as shown in Fig. 6. The wall pressure field is highly coherent for the unstable frequencies corresponding to the top of the peak and less coherent for frequencies on each side of it. Typically, the primary T–S waves are spanwise coherent over several centimeters, much more than turbulent eddies. The coherence decrease with increasing separation is approximately fit by exponentials, as shown in Fig. 9 for different frequencies. The corresponding correlation length is 160 mm for the dominant most amplified frequency and goes down to 10 mm at the peak sides. This part of the spectrum was found to be less coherent at higher flow velocity. More spectacular, the tones are almost perfectly correlated: The acoustic circular wave fronts produced at any point on the trailing edge force the T–S waves at point P to follow the same spanwise phase-lock, so that a few iterations of the feedback loop are enough to tune the instabilities over the whole span. Strictly speaking in that case, the statistical analysis is no longer valid, and a deterministic calculation should be performed to reproduce the interference that determines the far field. As a consequence, only the primary T–S radiation with no acoustic backreaction is retained in the present study.

Figure 8 also suggests that the difference between wall pressure and far-field spectra is smaller around the dominant frequency of the peak, which mainly corresponds to the most naturally amplified instability waves: A stronger emergence of the T–S broadband hump of the spectrum is seen in the acoustic signal than in the wall pressure signal. This will be confirmed later. The larger radiation efficiency is obviously related to the larger value of $l_y(\omega)$ obtained earlier. Frequencies away from the peak are poorly correlated. It can be assumed that this part of the spectrum tends to behave in the same way as a fine-scale turbulent boundary layer. The assumption of a correlation length much smaller than the span is evoked in the derivation of the formulations (1) and (2). This is not verified here because $l_y(\omega) \simeq L/2$ for the most unstable frequencies. The net expected effect is an overprediction of the noise level up to 4 dB, as pointed out by Casalino et al.[28] on the basis of numerical simulations in the similar case of the vortex shedding behind a circular cylinder. The value of l_y has then been corrected by these 4 dB in the following application of Sec. V as a first approximation.

C. Turbulent Vortex Shedding

At an angle of attack $\alpha_g = 5.5$ deg and all investigated values of the Reynolds number, the Valeo airfoil encounters flow conditions for which the boundary-layer thickness rapidly increases at the trailing edge on the suction side. This corresponds to a distributed constant shear, as confirmed by pitot tube measurements in a direction normal to the surface just downstream of the trailing edge. There is no mean reversed flow as would be the case if a full separation occured. Random vortex shedding is believed to take place in that case, the mean velocity remaining in the streamwise direction. Much a thinner, laminar, and stable boundary layer develops on the pressure side. This configuration is considered as the relevant one for a loaded fan blade. Because the boundary layer remains attached in the mean, this flow regime is referred to here as turbulent vortex shedding. A small laminar separation bubble is also observed at the leading edge. Both areas have been obtained by RANS computations[22] and confirmed by flow visualizations and convection speed measurements.

Wall pressure and far-field spectra are plotted in Fig. 10. Broadband radiation is generated as in the case of the turbulent boundary

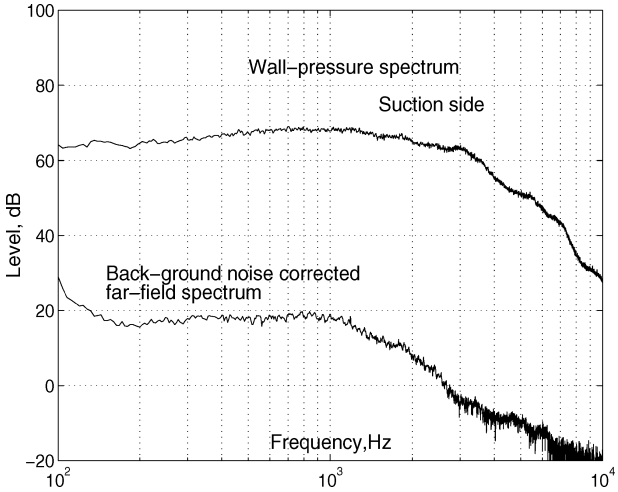

Fig. 10 Far-field and wall pressure spectra for the vortex shedding case, $\alpha_g = 5.5$ deg and $U_0 = 16$ m/s ($Re_c = 1.6 \times 10^5$).

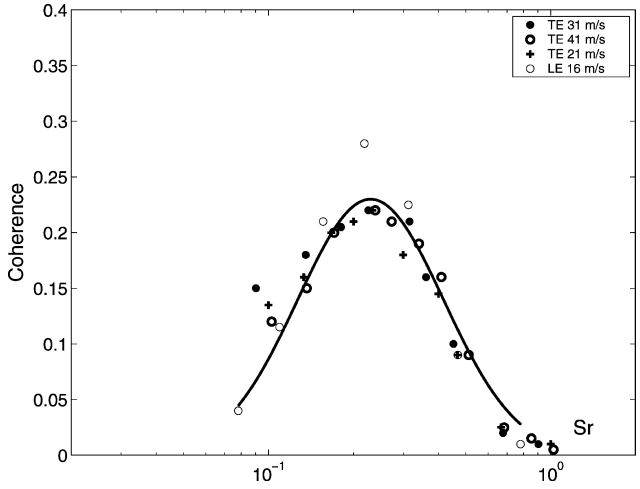

Fig. 11 Reduced coherence plots for the vortex shedding regime; Strouhal number based on separation thickness.

layer. However, the statistics of the wall pressure fluctuations and the resulting radiation spectral shape are different. As shown in Fig. 6, coherence plots exhibit a high-frequency bump. This feature suggests that the vortex shedding is almost coherent around some dominant frequency. Measurements have been performed at the same α_g but different flow speeds to confirm this behavior. For a given spanwise separation, the level of coherence is the same at all speeds, the bump being shifted toward higher frequencies as flow speed increases. When the coherence is plotted in Fig. 11 as a function of the Strouhal number based on the thickness of the suction side boundary layer at the trailing edge δ_S (about 7 mm here), an excellent agreement for collapse is obtained for all velocities. The peak coherence is achieved for a dominant Strouhal number of 0.22. Roughly speaking, this flow regime generates more noise around the vortex shedding frequency than would be produced by a bluff body with thickness δ_S. The difference is that the spectral spreading extends on a large frequency range, whereas the classical vortex shedding behind a bluff body is more concentrated at the Strouhal frequency. This can be attributed to the fact that the formation length and starting points of the shed vortices are not fixed on the airfoil surface. The characteristic scale δ_S is not as clearly defined as a physical body thickness. However, it appears as the leading parameter of the trailing-edge noise mechanism in this configuration. Practically, δ_S can be either evaluated by velocity measurements or deduced from RANS simulations. The convection speed has been evaluated again from the measured phase diagrams. A characteristic value $U_c = 0.67U_0$ has been found.

The evidence of a similar statistical behavior is found between streamwise probes near the reattachment area of the leading-edge separation bubble. The coherence bump occurs at significantly higher frequencies corresponding to smaller separation bubble thickness. Though laminar, the leading-edge separation generates vortices due to the oscillations of its shear layer, with the same statistical properties as the ones shed at the trailing edge. Moreover, when the bubble thickness deduced from RANS computations (around 2.5 mm here) is used as a characteristic dimension, the same dominant Strouhal number 0.22 is found. The corresponding plot is added for comparison in Fig. 11.

These results suggest that universal properties could be deduced for the vortical disturbances associated with separated or nearly separated flows on airfoils. The frequency content is distributed around a Strouhal number based on the thickness of the separated flow of 0.22 and extends over a Strouhal number range from 0.08 to 1. In the present case, the laminar leading-edge separation is not believed to contribute to the sound field because the reattachement is far from any surface singularity. Only the trailing-edge distributed vortex shedding is responsible for the radiated noise, due to the same scattering process as in the other cases. As seen in Fig. 11, the coherence has a Gaussian distribution on a logarithmic frequency scale. The following model fits the present results quite fairly:

$$\gamma^2(\eta, f) = A(\eta)\exp\left\{-75\left[\frac{\log_{10}(f)-\log_{10}(f_0)}{\log_{10}(f_0)}\right]^2\right\}$$

with $A(\eta) = \exp(-\eta/0.0025)$ and $f_0 = 0.22U_0/\delta_S$. This leads to a spanwise correlation length

$$l_y(\omega) = 0.005\exp\left\{-37.5\left[\frac{\log_{10}(f)-\log_{10}(f_0)}{\log_{10}(f_0)}\right]^2\right\} \quad (5)$$

The decoupling of frequency and sensor separation in this model should now be confirmed in other similar cases. Equation (5) holds for the frequency range associated with the main detached vortical eddies. Other values such as the usual ones for a turbulent boundary layer must be used out of this range.

V. Analytical Modeling

As noted in Sec. II, experimental results are first expressed in terms of a transfer function S_{pp}/Φ_{pp} that is then used to check the calculated radiation integral. This transfer function is plotted at the top of Fig. 12 for the three investigated flow regimes and an approximate observation angle of 80 deg with respect to the chord line. A nondimensional radiation ratio is defined by dividing this transfer function by the spanwise correlation length l_y and multiplying by R^2/L. The result is shown at the bottom of Fig. 12. A significant dispersion is observed on the values of the transfer function. The expected trend of a decrease with the inverse frequency for a fully developed turbulent boundary layer, according to Corcos's model,[18] is only partially found beyond 1 kHz. The turbulent boundary-layer configuration provides a low-efficiency radiation with a value of the transfer function around −55 dB. The turbulent vortex shedding regime is substantially more an efficient process, except at higher frequencies. The T–S waves regime corresponds to the highest value of the transfer function in the range of unstable frequencies (−46 dB) and the lowest outside of this range. For the same airfoil, all values of the radiation ratio should collapse. This is not exactly so here. However, a good collapse is obtained in the higher frequency range, between 500 Hz and 3 kHz. The radiation ratio is nearly constant, which is in a qualitative agreement with both Howe's formula and the theoretical result of Fig. 3 when the oscillations in the radiation integral are ignored.

The calculated values of the radiation ratio are also plotted in Fig. 3. Globally, both models provide the right orders of magnitude,

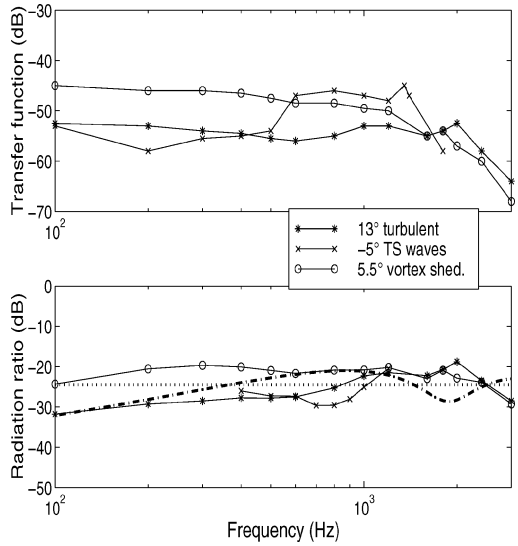

Fig. 12 Measured transfer function and radiation ratio, Valeo airfoil; comparison with theoretical results, $U_0 = 16$ m/s ($Re_c = 1.6 \times 10^5$): · · · ·, Eq. (1) and - · - ·, Eq. (2).

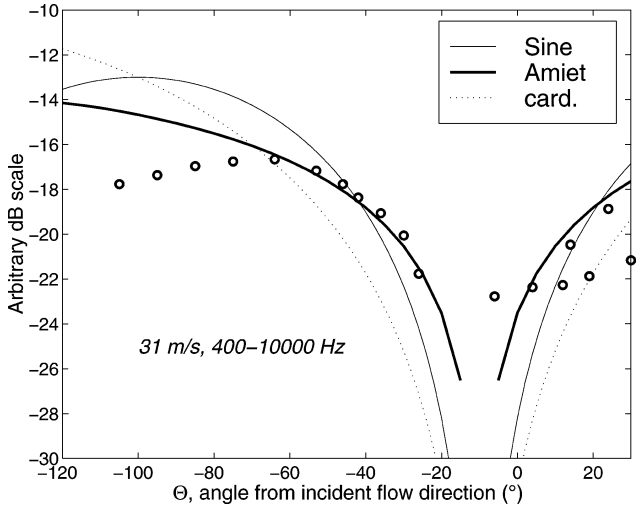

Fig. 13 Measured directivity patterns, with respect to the inlet flow direction, and calculated results; negative angles correspond to measuring points facing the pressure side.

except for discrepancies of a couple of decibels, depending on frequency. Furthermore, the results for the T–S waves regime suggest again that the radiation ratio is slightly underestimated when related directly to l_y, despite the statistical correction given in Sec. IV.B. The agreement found confirms that the far-field sound is nearly proportional to the wall pressure fluctuation amplitude close to the trailing edge multiplied by the spanwise correlation length. Remaining discrepancies might be partially attributed to the difficulty of measuring $l_y(\omega)$ and U_c precisely over the whole frequency range. For instance, as shown by numerical tests with the formula (2), a 15% decrease of U_c induces a typical 3-dB reduction of the radiation efficiency. Similarly, a 20% decrease of l_y induces a 1-dB reduction. Because the slope in the phase diagrams is not exactly constant, neither can be U_c. This is a possible origin of discrepancies. Furthermore, formula (2) is an approximation valuable at relatively large aspect ratios, whereas the actual aspect ratio is about 3 in the experiment. In that sense, the present results are understood as a preliminary assessment. Refined experiments, as well as additional computations on the basis of the extended formula detailed in Ref. 15, are a matter for a further investigation, still in progress.

Another explanation for the discrepancies is in the assumption of a full Kutta condition. Howe[6] pointed out that a partial unsteady Kutta condition at higher frequencies should increase the radiated noise. No correction has been attempted here because no indication of the degree of Kutta condition is available, on the one hand, and the correction is not straightforward in the Schwarzschild's technique, on the other hand.

Finally, directivity has been investigated in the case of the vortex shedding regime. The frequency integrated result is reported in Fig. 13 for a flow velocity of 31 m/s in an arbitrary decibel scale. Plots are shifted vertically with respect to each other for a comparison of relative variations with angle. The theoretical sinelike pattern associated with the point dipole and the cardioid pattern associated with the half-plane solution are first shown in Fig. 13. Both disagree with the present measurements, due to the noncompactness and the limited value of the chord length, respectively. Finally the calculated directivity pattern according to the present finite-chord model described by Eq. (2) is also plotted in Fig. 13. This finite chord result lies somewhere between the sine and cardioid, which can be considered as two opposite asymptotic trends. It provides a far better overall agreement. Remaining discrepancies might be attributed to the diffraction by the nozzle lips, which will be studied later on.

VI. Conclusions

An experiment dedicated to the study of airfoil self-noise at low Mach numbers has been performed. Self-noise radiation efficiency has been deduced by measuring a transfer function, defined as the ratio of the far-field acoustic pressure to the wall pressure close to the trailing edge and the statistical properties of the wall pressure field. Three flow regimes have been investigated on the same airfoil, for which the flow conditions are equivalent to a turbulent boundary layer, a vortex shedding regime, and an unstable laminar boundary layer with T–S waves. The turbulent boundary layer provides the less efficient mechanism, whereas the T–S wave regime provides the most efficient one. When scaled by dividing the transfer function by the spanwise correlation length, all data collapse reasonably, even though the spanwise correlation length can be obtained accurately only in a limited frequency range, as well as the convection speed used in the radiation integral. This suggests that all configurations can be analyzed using the same statistical approach.

An analytical model based on an extension of Amiet's theory has been used to account for all effects due to the finite chord length. It has been assessed against Howe's theory of the scattering by the edge of a half plane at low Mach number. Both formulations have been compared to the measurements. They provide the same order of magnitude within the range of flow speed and frequency covered by the experiment, at directions perpendicular to the flow. The main difference between the two formulations is in the directivity pattern: The half-plane theory cannot account for the vanishing radiation upstream of the leading edge, whereas the finite chord formulation does. Moreover, the latter is more consistent with the observed directivity diagrams. The proposed extension of Amiet's theory is, therefore, more convincing because it behaves favorably in terms of frequency distribution and directivity of the far-field sound. It is concluded that the wall pressure field can be used to infer the far-field sound, even if all of the details of the scattering mechanism, such as the Kutta condition, are not fully understood. Despite the remaining discrepancies between theory and experiment, the formulation can help to estimate fan broadband self-noise in an industrial context, until a better prediction is available at a reasonable cost using computational aeroacoustics. The practical need for flow input data is another important matter if noise predictions are included in a design process. A minimum statistical description of the velocity field can be extracted from the existing RANS methods but not the required wall pressure parameters. LES methods could provide the required data, but they are still far from an easy and daily use for designers. The development of extra analytical models, relating for instance the statistics of the velocity field to the one of the pressure field in basic cases, is an alternative way to be explored. The characteristic Strouhal number of 0.22 found for a separated bubble thickness, or the vortex shedding thickness of a loaded airfoil, is another example of the possible use of RANS methods to infer broadband noise: The averaged computation of the thickness allows the prediction of the frequency range and the value of the maximum spanwise correlation length.

References

[1]Blake, W. K., "A Statistical Description of Pressure and Velocity Fields at the Trailing Edge of a Flat Strut," David Taylor Naval Ship Research and Development Center, DTNSRD Rept. 4241, Bethesda, MD, Dec. 1975.

[2]Brooks, T. F., and Hodgson, T. H., "Trailing-Edge Noise Prediction from Measured Surface Pressures," *Journal of Sound and Vibration*, Vol. 78, No. 1, 1981, pp. 69–117.

[3]Garcia, P., and Gérard, P., "Bruit d'un Profil dans un Écoulement," ONERA, TP 1984-155, Chatillon, France, Nov. 1984; also *La Recherche Aérospatiale*, English version, Vol. 3, 1989, pp. 1–7.

[4]Ffowcs Williams, J. E., and Hall, L. H., "Aerodynamic Sound Generation by Turbulent Flow in the Vicinity of a Scattering Half-Plane," *Journal of Fluid Mechanics*, Vol. 40, 1970, pp. 657–670.

[5]Amiet, R. K., "Noise Due to Turbulent Flow past a Trailing Edge," *Journal of Sound and Vibration*, Vol. 47, No. 3, 1976, pp. 387–393.

[6]Howe, M. S., "A Review of the Theory of Trailing-Edge Noise," *Journal of Sound and Vibration*, Vol. 61, No. 3, 1978, pp. 437–465.

[7]Wang, M., and Moin, P., "Computation of Trailing-Edge Flow and Noise Using Large-Eddy Simulation," *AIAA Journal*, Vol. 38, No. 12, 2000, pp. 2201–2209.

[8]Manoha, E., Delahay, C., Sagaut, P., Mary, I., Ben Khelil, S., and Guillen, P., "Numerical Prediction of the Unsteady Flow and Radiated Noise from a 3D Lifting Airfoil," AIAA Paper 2001-2133, May 2001.

[9]Manoha, E., Herrero, C., Sagaut, P., and Redonnet, S., "Numerical Prediction of Airfoil Aerodynamic Noise," AIAA Paper 2002-2573, June 2002.

[10]Ewert, R., Meinke, M., and Schröder, W., "Computation of Trailing Noise via LES and Acoustic Perturbation Equations," AIAA Paper 2002-2467, June 2002.

[11]Manoha, E., Troff, B., and Sagaut, P., "Trailing-Edge Noise Prediction Using Large-Eddy Simulation and Acoustic Analogy," *AIAA Journal*, Vol. 38, No. 4, 2000, pp. 575–583.

[12]Singer, B. A., Brentner, K. S., Lockard, D. P., and Lilley, G., "Simulation of Acoustic Scattering from a Trailing Edge," AIAA Paper 99-0231, Jan. 1999.

[13]Manoha, E., Elias, G., Troff, B., and Sagaut, P., "Towards the Use of Boundary Element Method in Computational Aeroacoustics," AIAA Paper 99-1980, May 1999.

[14]Howe, M. S., "Edge-Source Acoustic Green's Function for an Airfoil of Arbitrary Chord, with Application to Trailing-Edge Noise," *Quarterly Journal of Mechanics and Applied Mathematics*, Vol. 54, No. 1, 2001, pp. 139–155.

[15]Roger, M., Moreau, S., and Wang, M., "Towards Airfoil Self Noise Prediction Using Wall-Pressure Statistics from LES and an Analytical Acoustic Model," *Center for Turbulence Research Annual Research Briefs*, Stanford Univ./NASA Ames Research Center, Stanford, CA, 2002, pp. 405–414.

[16]Amiet, R. K., "Acoustic Radiation From an Airfoil in a Turbulent Flow," *Journal of Sound and Vibration*, Vol. 41, No. 4, 1975, pp. 407–420.

[17]Sabah, M., and Roger, M., "Experimental Study and Model Predictions of Cascade Broadband Noise," AIAA Paper 2001-2243, May 2001.

[18]Corcos, G. M., "The Structure of Turbulent Pressure Field in Boundary-Layer Flows," *Journal of Fluid Mechanics*, Vol. 18, 1964, pp. 353–378.

[19]Roger, M., and Moreau, S., "Trailing Edge Noise Measurements and Prediction for Subsonic Loaded Fan Blades," AIAA Paper 2002-2460, June 2002.

[20]Pérennès, S., and Roger, M., "Aerodynamic Noise of a Two-Dimensional Wing with High-Lift Devices," AIAA Paper 98-2338, June 1998.

[21]Brooks, T. F., Marcolini, M. A., and Pope, D. S., "Airfoil Self-Noise and Prediction," NASA RP-1218, July 1989.

[22]Moreau, S., Iaccarino, G., Roger, M., and Wang, M., "CFD Analysis of Flow in an Open-Jet Aeroacoustic Experiment," *Center for Turbulence Research Annual Research Briefs*, Stanford Univ./NASA Ames Research Center, Stanford, CA, 2001, pp. 343–351.

[23]Amiet, R. K., "Refraction of Sound by a Shear Layer," *Journal of Sound and Vibration*, Vol. 58, No. 4, 1978, pp. 467–482.

[24]Arbey, H., and Bataille, J., "Noise Generated by Airfoil Profiles Placed in a Uniform Laminar Flow," *Journal of Fluid Mechanics*, Vol. 134, 1983, pp. 33–47.

[25]Paterson, R. W., Vogt, P. G., Fink, M. R., and Munch, C. L., "Vortex Noise of Isolated Airfoils," *Journal of Aircraft*, Vol. 10, No. 5, 1973, pp. 296–302.

[26]McAlpine, A., Nash, E. C., and Lowson, M. V., "On the Generation of Discrete Frequency Tones by the Flow Around an Aerofoil," *Journal of Sound and Vibration*, Vol. 222, No. 5, 1999, pp. 753–779.

[27]Tam, C. K. W., "Discrete Tones of Isolated Airfoils," *Journal of the Acoustical Society of America*, Vol. 55, No. 6, 1974, pp. 1173–1177.

[28]Casalino, D., and Jacob, M., "Prediction of Aerodynamic Sound from Circular Rods via Spanwise Statistical Modeling," *Journal of Sound and Vibration*, Vol. 262, 2003, pp. 815–844.

W. J. Devenport
Associate Editor